

Variation of the sunspot area during the rising and declining phases of the solar cycle supports the toroidal flux loss due to flux emergence

Bidya Binay Karak,¹★ Soumya Mishra,² Anu Sreedevi¹

¹Department of Physics, Indian Institute of Technology (Banaras Hindu University), Varanasi 221005, India

²School of Physical Sciences, National Institute of Science Education and Research Bhubaneswar, Jatni, Khurda 752050, India

Accepted XXX. Received YYY; in original form ZZZ

ABSTRACT

Sunspots are obvious observable manifestations of the toroidal magnetic field generated through the dynamo in the convection zone. They appear in different sizes, having a wide distribution in their area. We analyse the sunspot group area of the past 13 cycles and the Bipolar Magnetic Region (BMR) flux for Cycles 23 and 24 to explore their area and flux distributions and connect with the theory. We find that, in general, the group area and BMR flux are statistically larger in the rising phase than in the declining phase of the solar cycle. This implies that the rising phase of the solar cycle is prone to drive more intense space weather. We further show that the mean and median of the area distribution during the rising phase are dependent on cycle strength. However, the distribution mean and median are cycle strength-independent or weakly dependent during the decline phases of the solar cycles, particularly during the last three years when the latitudinal bands of all cycles migrate towards the equator along the same trajectory. These results support the theoretical model of nonlinear flux loss due to flux emergence, which explains why solar cycles rise differently but decay similarly.

Key words: Sun: activity – (Sun:) sunspots – Sun: magnetic fields – Sun: interior – Sun: photosphere

1 INTRODUCTION

Although the amplitude of the solar cycle varies irregularly from one cycle to another, its amplitude can be predicted if the cycle has progressed a few years after the minimum by computing its rise rate (Kane 2008; Kumar et al. 2022). This is due to the existence of a robust relationship, popularly known as the Waldmeier effect (Waldmeier 1935). The classical form of this effect states that a strong cycle takes less time to rise, while a weaker one takes longer (Hathaway et al. 2002). Due to irregular variations of solar activity within a cycle (short-term fluctuations like quasi-biannual oscillations, and double peaks), it becomes inaccurate to determine the exact times of solar minimum and maximum (and thus the rise time) and the cycle amplitude, making it sometimes difficult to establish the Waldmeier Effect in the solar cycle (Dikpati et al. 2008; Garg et al. 2019). However, if the rise rate instead of the rise time is taken, then the Waldmeier Effect is robustly reproduced in all proxies of the solar cycle data (Cameron & Schüssler 2008; Karak & Choudhuri 2011).

Waldmeier (1955) studied Waldmeier Effect in a slightly different way. He analyzed the migration of the latitudinal distribution of sunspots in each cycle. He showed that as the activity level (e.g., number of sunspots) increases, the parameters (centres and widths) of the butterfly wings of different cycles evolve at different rates as the sunspot latitudes migrate towards the equator. However, when the activity level declines, the parameters of the butterfly wing evolve in the same way for all cycles (see Figs. 3–4 of Cameron & Schüssler 2016).

Biswas et al. (2022) explained this feature using a nonlinear loss of toroidal flux due to magnetic buoyancy in the dynamo model. They employed the algorithm of Nandy & Choudhuri (2001, 2002) to capture the toroidal flux from the base of the convection zone (CZ) to the surface in the form of sunspots in the following way: If the toroidal field in any grid above the base of CZ exceeds a certain threshold B_c (which was determined to be 10^4 G), then a fraction of the flux is emerged by simply reducing this flux at that grid point and by adding the same flux on the surface. Hence, two processes of the toroidal flux determine the cycle phase: the generation/supply and the loss through flux eruptions. In the rising phase of a cycle, the generation dominates over the loss, keeping the toroidal field well above B_c . This results in a rapid increase in the sunspot number in the early phase. However, rapid spot eruption increases the flux loss, and at some point the flux loss dominates the generation, reducing the field close to B_c . The cycle no longer grows. Any new generation of flux is compensated by eruptions, and the model continues to produce spots as the cycle decays, maintaining the field near B_c . In a strong cycle, the toroidal field is high, and spots erupt more frequently. However, this frequent spot eruption rapidly reduces the toroidal field to near B_c , and the cycle begins to decline early. For a weak cycle, the situation is different. It produces spots less frequently, and the activity level grows slowly. The toroidal flux loss is lower, and the cycle grows slowly for a long time; by then, the activity level moves a bit closer to the equator (compared to a strong cycle, which begins to decline when the activity level is already at high latitude). Eventually, when a sufficient amount of flux is lost, the toroidal field becomes comparable to B_c , and the weak cycle also begins to decline at the same rate as the strong cycle.

If the above explanation, as detailed in Biswas et al. (2022), holds

★ E-mail: karak.phy@iitbhu.ac.in (BBK)

in the Sun, we expect the sunspot properties, such as magnetic field and flux, in the declining phase to be of similar strength, while in the rising phase, they will be cycle dependent (stronger cycles are expected to have bigger spots). However, the magnetic field observed on the solar cycle has weak or no resemblance to the field that had erupted from the deep CZ (due to various processes during the rise through the surface layer; [Cheung & Isobe 2014](#)). Furthermore, the magnetic field information of the sunspot is not reliable due to measurement issues before 1996 and is limited to only the last three cycles from space based observations ([Ulrich et al. 2002](#); [Scherrer et al. 1995](#); [Watson et al. 2011](#); [Schou et al. 2012](#)). Therefore we should not consider the magnetic field to check the solar cycle phase dependence of the sunspot properties to connect this theory. The sunspot flux for which we have the systematic records from space-based data (from the Michelson Doppler Imager (MDI) on board the Solar and Heliospheric Observatory (SOHO) and Helioseismic and Magnetic Imager (HMI) on board the Solar Dynamic Observatory (SDO)) are available for the last two solar cycles. However, the sunspot area—a good proxy of the flux of the sunspot ([Schrijver & Harvey 1994](#); [Sakurai & Toriumi 2023](#))—can be resembled to the magnetic flux of the sunspot forming flux tubes¹, and the records of the sunspot area have been available for several cycles. Fortunately, [Mandal et al. \(2020\)](#) cross-calibrated the sunspot records from various observatories and produced homogeneous data for the last 13 solar cycles. Therefore, we shall consider the sunspot area during the different phases of the solar cycle and check if there is any variation in different phases, to support the theory of the solar cycle as given in [Biswas et al. \(2022\)](#). Our results will also point out that the two phases of the solar cycle, namely the rising and declining phases, do not contribute equally to driving the space weather.

2 DATA AND METHODOLOGY

We analyze the cross-calibrated and homogeneous catalog of individual corrected sunspot group areas spanning 1874–2025 compiled by [Mandal et al. \(2020\)](#), which combines measurements from the Royal Greenwich Observatory (RGO), Kislovodsk, Pulkovo, and Debrecen observatories. Since sunspot group catalogs do not contain direct magnetic information, we use space-borne magnetograms from MDI/SOHO (for Cycle 23) and HMI/SDO (Cycle 24). For this purpose, we employ the catalog of Automatic Tracking Algorithm for Bipolar Magnetic Regions (AutoTAB; [Sreedevi et al. 2023](#)), which automatically detects and tracks the evolution of bipolar magnetic structures throughout their near-side lifetime. For each BMR, a representative flux value is assigned as the mean of the top 80% of its maximum flux during its evolution.

Individual cycles are identified from one sunspot minimum to the next using the yearly International Sunspot Number (ISN) Version 2.0 provided by WDC–SILSO, Royal Observatory of Belgium. To minimize contamination due to cycle overlap, one year at the beginning and one year at the end of each cycle are excluded from the analysis.

For each cycle, we compute the yearly sunspot number and the mean unsigned latitude of sunspot groups. The variation of these quantities for all cycles is shown in Figure 1. Let $S(t)$ denotes the annualized sunspot number. For a given cycle k with start year $t_0^{(k)}$

¹ While there is no direct theoretical or observational proof of this assumption, several independent studies support this reasoning (e.g., [Fisher et al. 1995](#); [Weber et al. 2013](#); [Cameron et al. 2018](#); [Cameron & Jiang 2019](#); [Chatterjee & Hazra 2025](#)).

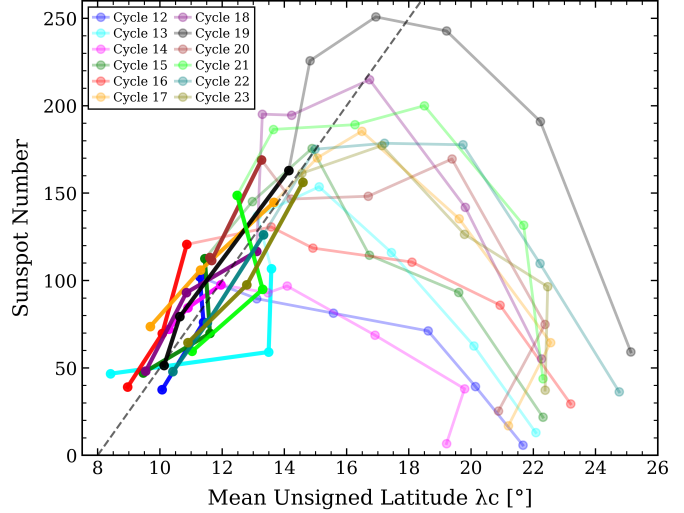


Figure 1. The mean of the absolute latitudes of sunspot groups in each year (λ_c) versus the number of sunspot groups in that year. Different curves are for different cycles. One year data at the beginning and at the end of each cycle are excluded in this analysis. Note that a cycle begins with a high value of λ_c on the right side of the plot and with the progress of a cycle when sunspot latitude band migrates equatorward, the trajectory moves towards the left. The dashed line (having sunspot number = $25\lambda_c - 200$) guides the uniform decay of all cycles. The dark parts of the curves highlight the last three years of each cycle during which all cycles fall at the same rate.

and end year $t_E^{(k)}$, we define the transition year $t_R^{(k)}$ as the year within the interval $[t_0^{(k)}, t^{(k)}]$ for which $S(t)$ attains its maximum. The rising phase is defined as the interval from $t_0^{(k)}$ to $t_R^{(k)} - 1$, while the declining phase extends from $t_R^{(k)} + 1$ to $t^{(k)}$. The transition year itself is treated as a discrete boundary and is excluded from both phases.

For most cycles, the phase boundaries determined using the yearly ISN are consistent with those inferred independently from the evolution of sunspot area and mean latitude in Figure 1. In several cycles (notably Cycles 14 and 22), the activity exhibits double peak around the solar maximum ([Karak et al. 2018](#)). In such cases, we adopt the year corresponding to the latter maximum of the yearly mean sunspot number as $t_R^{(k)}$. This choice reflects the sustained high activity level following the first peak and avoids an artificially early termination of the rising phase. This consideration is particularly important for strong cycles (notably Cycles 18, 19, 21), which are characterized by a rapid early rise followed by an extended period of elevated activity near maximum. Selecting the later peak as $t_R^{(k)}$ ensures that the rising-phase statistics are not biased by the unusually fast initial growth of strong cycles and yields a physically consistent separation between the rising and declining phases across cycles of different strengths.

3 RESULTS AND DISCUSSION

Isolating the sunspots for the rising and declining phases of all past 13 cycles, we study their properties. In Figure 2 we show the distribution of all sunspot group areas during the rising and declining phases, combined for all cycles. Here, we present the distribution from the daily total area data instead of the individual group area, as the latter distribution is somewhat noisy, and the two profiles are not distinctly visible. In Figure 2, we clearly identify two distinct

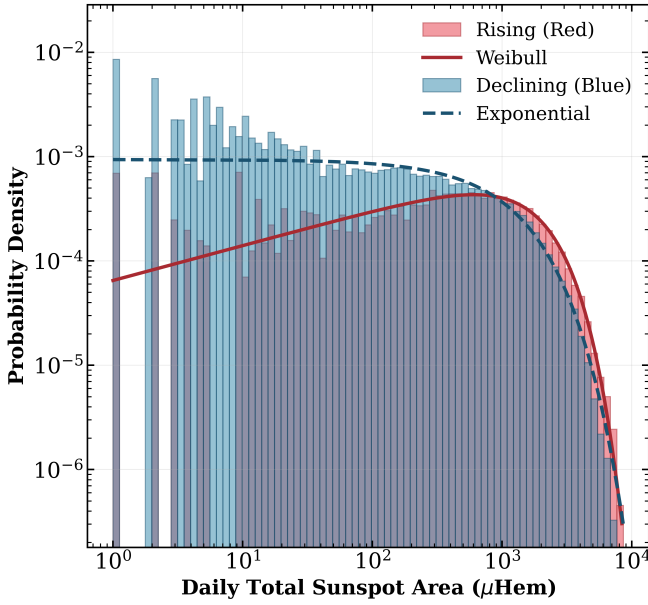


Figure 2. Distributions of the daily total sunspot areas (in μHem) during the rising (red) and declining (blue) phases of the solar cycle. The rising-phase distribution is best fitted by a Weibull function ($k = 1.335 \pm 0.010$, $\lambda = 1703.14 \pm 12.42 \mu\text{Hem}$), while the declining-phase distribution is better described by an exponential model ($\lambda = (9.36 \pm 0.06) \times 10^{-4} \mu\text{Hem}^{-1}$).

distributions corresponding to the rising and declining phases. The rising phase shows somewhat narrow distribution with peak at higher area value, while the distribution during the decline phase is peaking at a slightly lower area and has extended tail towards the lower value. The distribution corresponding to the declining phase is not described well by the log-normal but by the Weibull distribution. These behaviours clearly suggest that the rising phase of the solar cycle is distinct from the decline phase. This we explore in detail below by analysing the distribution properties separately for all the cycles.

The mean and median values of the area of all individual sunspot groups during the declining phases versus rising phases, computed separately for Cycles 12–24, are shown in Figure 3. Several inferences can be made from this plot. For most of the cycles (except Cycles 15, 21, and 23² for the mean and Cycles 14–17 for median), the mean or median value of the sunspot area during the rising phase is higher than that of the decline phase. This is consistent with the results presented in the area distribution in two phases, combined for all cycles (Figure 2; also see the distributions of the daily sunspot area in Figure A1 for a few cycles). This clearly implies that the Sun produces (statistically) bigger spots during the rising phase than in the decline phase. Observations indeed find that the intensity of the solar flare eruptions increases with the group area, although the complexity of the magnetic structure plays a key role (Sammis et al. 2000; Ternullo et al. 2006; Lee et al. 2012; Watari 2022; Lin et al. 2023; Kumar et al. 2025). Consequently, the rising phases are prone to drive more violent space weather. Another point is that the data points are not strongly correlated in this plot. This implies

² For this cycle, sunspot properties extracted from the SOHO/MDI data also do not show significantly lower values in the declining phase than those in the rising phase (Watson et al. 2011).

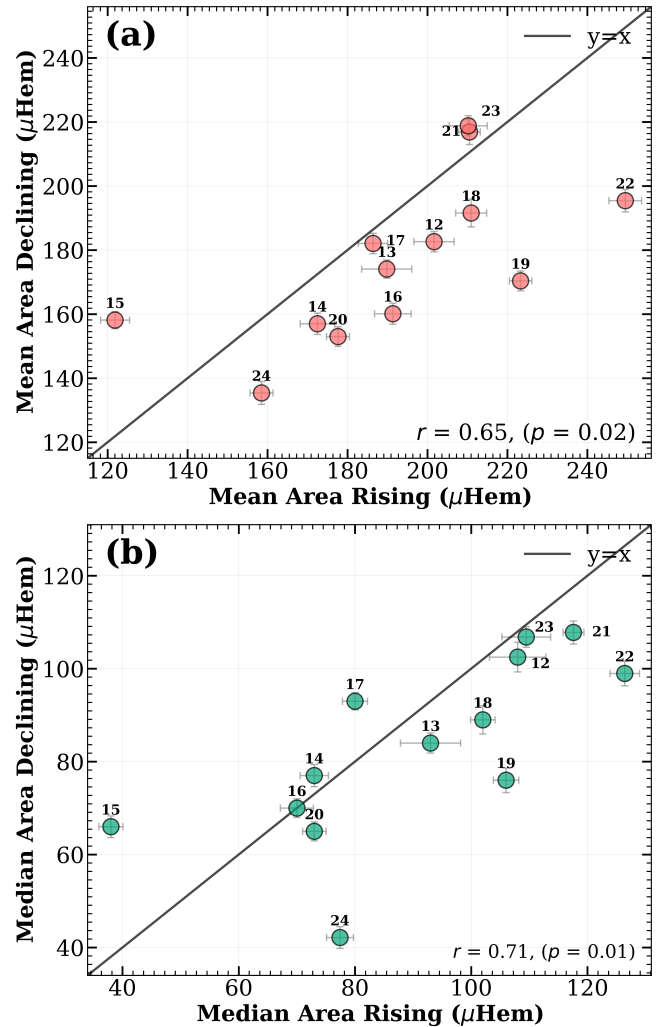


Figure 3. Scatter plots of the (a) mean and (b) median area of sunspot groups computed over the rising phase versus the same over the decline phase. Cycle numbers are assigned to each data points. The linear Pearson correlation coefficients (r) and p values are printed on each subplot.

that if the sunspot area during the rising phase is large, then it is not necessary that the spot area during the decline phase will also be large. For example, Cycle 19 (which is one of the strongest cycles) has a considerably large value of the mean/median sunspot area during the rising phase, compared to its decline phase. This asymmetry in the sunspot area is high in the strong cycles and less in weak cycles (e.g., Cycles 12–16). Finally, the mean (or median) area during the rising phase (horizontal axis of this plot) have a larger variation than the area during the decline phase (the vertical axis). This suggests that the sunspot area during the decline phase is less dependent on the cycle strength.

To further explore this feature, we show the scatter plots of the mean and median areas during the rising and falling phases with the cycle strength in Figure 4. Here, the cycle strength is measured as the total area covered by the sunspot groups in the cycle. Instead of total area, if we consider the peak ISN sunspot number as the cycle strength, then also we get similar results. We note that in general the (mean and median) sunspot area is correlated with the cycle strength, suggesting that if a cycle is strong, it produces (statistically) bigger

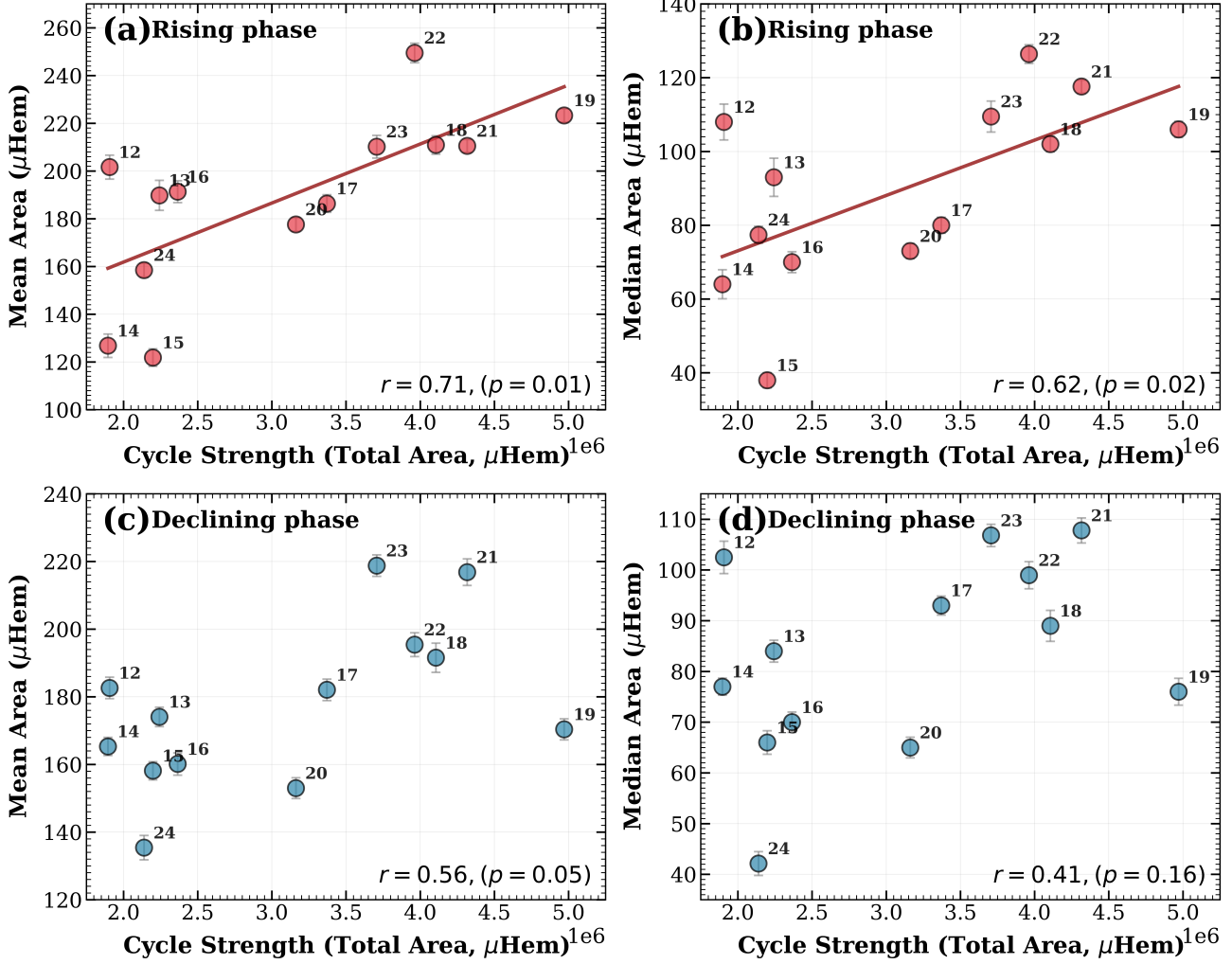


Figure 4. Top two panels: Mean area of sunspot groups during the (a) rising phase and (b) declining phase versus the cycle strength (measured by the total group area in μHem) for Solar Cycles 12–24. Points are labelled by the cycle number. The dashed line represents the best linear fit to the data. The bottom two panels are the same as the top ones, but for the median area. The linear Pearson correlation value and p are printed on each panel. The Spearman rank correlation coefficients for the four panels are 0.71 ($p = 0.01$), 0.62 ($p = 0.02$), 0.56 ($p = 0.05$), and 0.41 ($p = 0.16$), respectively.

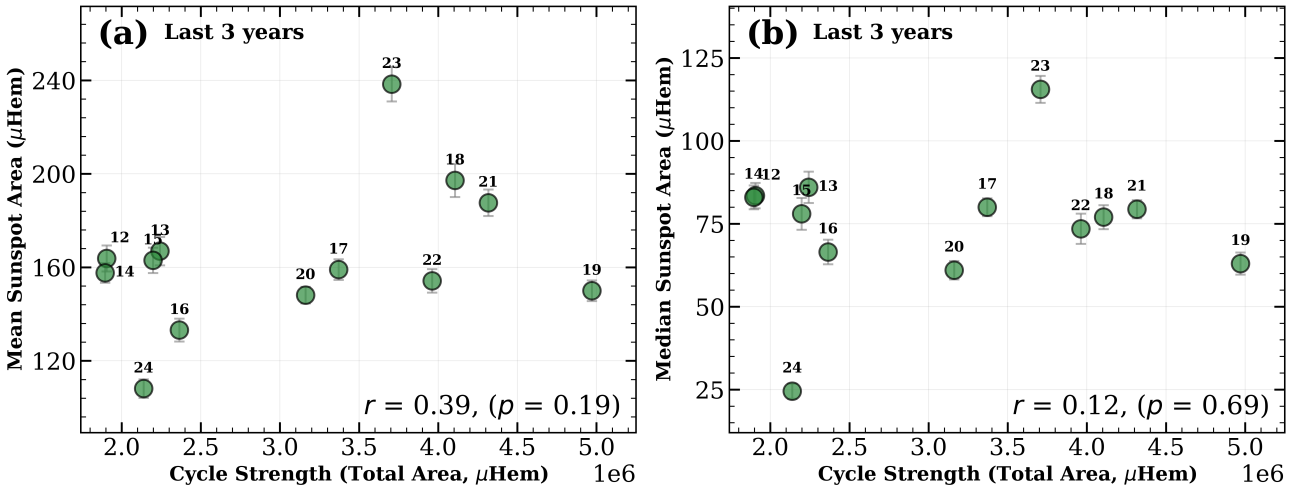


Figure 5. The same as the bottom panels of Figure 4 but from the sunspot areas during the last 3 years (excluding the final year) of the decline phase of the cycle.

spots, consistent with the results of sunspots from the Kodaikanal Solar Observatory (Mandal & Banerjee 2016). This is also the reason why strong cycles are more prone to produce extreme space weather events (Chapman et al. 2020; Owens et al. 2021). However, the correlation between the sunspot area (mean and median) with the cycle strength during the declining phase is less compared to that of during the rising phase.³ Again, this hints towards the fact that the decline phase is less correlated with the cycle strength.

This feature becomes more transparent when we consider only the sunspot area of the last three years (again we exclude one year at the end). In Figure 5, we observe that the mean and median sunspot areas over the last three years of the cycle are not correlated with the strength of the cycle. We find consistently similar results with the RGO (Greenwich - USAF/NOAA) data as well (Appendix A2).

Recalling the theory of Biswas et al. (2022), we know that the activity levels of all cycles fall at the same rate, and in particular the strong cycles begin to decline early (when the activity belt is already at high latitudes) and the weak cycles decline later. As highlighted in Cameron & Schüssler (2016) and in our Figure 1, we find that in the last few years of the cycles all the trajectories (of the activity vs latitude plane) are merged into a common trajectory. Clearly, this is the phase when the toroidal field at the base of the CZ remains comparable in all cycles and does not depend on the cycle strength. This is what is indicative here in Figure 5. While we are not observing a strictly constant value for the mean and median sunspot area, which we should not because of their statistical variations form a limited number and observational issues, we clearly observe them as cycle uncorrelated and the spread of the vertical-axes of Figure 5 is quite small. Although the values for Cycles 23 and 24 are deviated from the average trend, shifting the 3-year window by one year towards the weaker / intense phase for Cycle 23/24 helps reduce the spread in Figure 5.

We note that there is an equally promising alternative explanation for the uniform decay of cycles, as given by Cameron & Schüssler (2016) and later explored in a dynamo model by Talafha et al. (2022), based on diffusive cancellation at the equator. However, in this scenario, the decline phase will still be cycle-dependent; strong cycles are expected to have high flux spots even in their decline phase. In observations (Figure 4 bottom panels and Figure 5), we find that even strong cycles (e.g., Cycle 19) do not have a higher sunspot area; all cycles have more or less similar sunspot area. Hence, based on our understanding, this diffusive cancellation idea does not seem to be a favourable explanation for the observed properties of solar cycle decay. However, future studies are required to confirm this.

Finally, as discussed earlier, we also check the cycle phase dependence of sunspots with LOS magnetic observations from AutoTAB for Cycles 23 and 24. During the rising phase of Cycle 23/24, the mean magnetic fluxes are $5.47 \times 10^{23} \pm 1.9 \times 10^{21}$ / $(1.12 \times 10^{23} \pm 5.08 \times 10^{20})$ Mx, while the corresponding median values are 1.5×10^{22} / 1.1×10^{22} Mx. In the declining phase, the mean flux values for Cycle 23/24 are $3.04 \times 10^{23} \pm 8.9 \times 10^{20}$ / $1.21 \times 10^{22} \pm 1.5 \times 10^{19}$ Mx with median values of 1.34×10^{22} / 3.12×10^{21} Mx, respectively. We note that the AutoTAB catalog includes not only sunspot-forming regions, but also weaker BMRs that do not appear as sunspots, as well as some high-flux ephemeral regions (Sreedevi et al. 2024). Interestingly, the higher mean and median flux values observed during the rising phase are reflected not only in sunspot data but also in the broader BMR population,

³ If we include the transition year in the rising phase of the cycle, then the correlations in panels (a) and (b) of Figure 4 improve slightly.

highlighting a consistent magnetic signature across different scales of flux emergence.

4 CONCLUSION

We have provided pieces of observational evidence behind the theory of Biswas et al. (2022), which explained a fundamental feature of the solar cycle: Different cycles rise at different rates while their decline phase is similar (Waldmeier 1955; Cameron & Schüssler 2016). They employed the buoyancy algorithm of Nandy & Choudhuri (2001, 2002) in solar dynamo, namely, when the toroidal magnetic field in the CZ exceeds a certain threshold, a fraction of the toroidal flux is released from there to form a sunspot on the solar surface. Using this idea, Biswas et al. (2022) showed that in the early phase of the solar cycle, the toroidal field is considerably higher than this threshold, allowing the cycle to grow fast. As every sunspot eruption releases some flux, the Sun releases a considerable amount of flux during the early phase of the solar cycle, bringing the field down to the threshold, causing the cycle to decline. This flux loss happens at a faster rate for a strong cycle, causing the cycle to decline early when the activity belt is already at high latitudes (compared to a weak cycle, whose flux loss occurs at a slow rate and the toroidal belt at the base of the CZ is advected towards the equator). Thus, during the rising phase of the solar cycle, we expect large spots, and they should correlate with the cycle strength. In contrast, for the decline phase (at least for the last three years when all cycles decline in the same way), since the field in the CZ is comparable to the threshold, we expect small spots and sunspot properties to be cycle-independent. By analysing the areas of the sunspot groups for the last 13 solar cycles and BMRs from LOS magnetograms from the last two cycles, we find general agreement with the expectation from the above theory. In particular, we find that (i) the distribution of sunspot group areas of the rising phase is shifted towards higher values compared to that of the decline phase and (ii) the mean and median values of the sunspot areas during the rising phase are correlated with the cycle strength, while the decline phase of the area distribution is largely uncorrelated with the cycle strength. Our analysis also suggests that the rising phase of a cycle is prone to cause more intense space weather.

ACKNOWLEDGEMENTS

The authors sincerely thank the reviewer for offering several constructive comments and questions; answering them helps improve the quality of the article. The authors also are indebted to Robert Cameron for a helpful discussion and suggestion. B.B.K. acknowledges the financial support from the Anusandhan National Research Foundation (ANRF) through the MATRIC program (file no. MTR/2023/000670).

DATA AVAILABILITY

Sunspot area data were obtained from Mandal et al. (2020) who produced cross-calibrated and corrected areas of individual sunspot groups during 1874–2025, and from Royal Observatory, Greenwich - USAF/NOAA Sunspot Data. The International Sunspot Number V2.0 is obtained from WDC-SILSO, Royal Observatory of Belgium, Brussels. AutoTAB catalog is available at <https://github.com/sreedevi-anu/AutoTAB>

REFERENCES

Biswas A., Karak B. B., Cameron R., 2022, *Phys. Rev. Lett.*, **129**, 241102

Cameron R. H., Jiang J., 2019, *A&A*, **631**, A27

Cameron R., Schüssler M., 2008, *ApJ*, **685**, 1291

Cameron R. H., Schüssler M., 2016, *A&A*, **591**, A46

Cameron R. H., Duvall T. L., Schüssler M., Schunker H., 2018, *A&A*, **609**, A56

Chapman S. C., Horne R. B., Watkins N. W., 2020, *Geophys. Res. Lett.*, **47**, e86524

Chatterjee S., Hazra G., 2025, *arXiv e-prints*, p. arXiv:2509.23959

Cheung M. C. M., Isobe H., 2014, *Living Reviews in Solar Physics*, **11**, 3

Dikpati M., Gilman P. A., de Toma G., 2008, *ApJ*, **673**, L99

Fisher G. H., Fan Y., Howard R. F., 1995, *ApJ*, **438**, 463

Garg S., Karak B. B., Egeland R., Soon W., Baliunas S., 2019, *arXiv e-prints*, p. arXiv:1909.12148

Hathaway D. H., Wilson R. M., Reichmann E. J., 2002, *Sol. Phys.*, **211**, 357

Kane R. P., 2008, *Journal of Atmospheric and Solar-Terrestrial Physics*, **70**, 1533

Karak B. B., Choudhuri A. R., 2011, *MNRAS*, **410**, 1503

Karak B. B., Mandal S., Banerjee D., 2018, *ApJ*, **866**, 17

Kumar P., Biswas A., Karak B. B., 2022, *MNRAS*, **513**, L112

Kumar R., Chandra R., Pande B., Pande S., 2025, *Indian Journal of Physics*, **99**, 3593

Lee K., Moon Y.-J., Lee J.-Y., Lee K.-S., Na H., 2012, *Sol. Phys.*, **281**, 639

Lin J., Wang F., Deng L., Deng H., Mei Y., Zhang X., 2023, *ApJ*, **958**, 1

Mandal S., Banerjee D., 2016, *ApJ*, **830**, L33

Mandal S., Krivova N. A., Solanki S. K., Sinha N., Banerjee D., 2020, *A&A*, **640**, A78

Nandy D., Choudhuri A. R., 2001, *ApJ*, **551**, 576

Nandy D., Choudhuri A. R., 2002, *Science*, **296**, 1671

Owens M. J., Lockwood M., Barnard L. A., Scott C. J., Haines C., Macneil A., 2021, *Sol. Phys.*, **296**, 82

Sakurai T., Toriumi S., 2023, *ApJ*, **943**, 10

Sammis I., Tang F., Zirin H., 2000, *ApJ*, **540**, 583

Scherrer P. H., et al., 1995, *Sol. Phys.*, **162**, 129

Schou J., et al., 2012, *Sol. Phys.*, **275**, 229

Schrijver C. J., Harvey K. L., 1994, *Sol. Phys.*, **150**, 1

Sreedevi A., Jha B. K., Karak B. B., Banerjee D., 2023, *arXiv e-prints*, p. arXiv:2304.06615

Sreedevi A., Jha B. K., Karak B. B., Banerjee D., 2024, *ApJ*, **966**, 112

Talafha M., Nagy M., Lemerle A., Petrovay K., 2022, *A&A*, **660**, A92

Ternullo M., Contarino L., Romano P., Zuccarello F., 2006, *Astronomische Nachrichten*, **327**, 36

Ulrich R. K., Evans S., Boyden J. E., Webster L., 2002, *ApJS*, **139**, 259

Waldmeier M., 1935, *Astronomische Mitteilungen der Eidgenössischen Sternwarte Zurich*, **14**, 105

Waldmeier M., 1955, *Ergebnisse und Probleme der Sonnenforschung* (Leipzig: Geest & Portig),

Watari S., 2022, *Earth, Planets and Space*, **74**, 115

Watson F. T., Fletcher L., Marshall S., 2011, *A&A*, **533**, A14

Weber M. A., Fan Y., Miesch M. S., 2013, *Sol. Phys.*, **287**, 239

APPENDIX A: SUPPORTING MATERIALS

A1 Distribution of sunspot area of individual cycles

As different cycles have different mean and median values of the sunspot area, the combined distribution of all sunspots does not reflect the true properties of the sunspot area for the rising and declining phases of the individual cycles. Therefore, here in Figure A1 we show the distributions of the daily sunspot areas of rising and declining phases from a few representative cycles.

A2 Cross-checking results using RGO data

So far in the above analyses, we have used the sunspot area data from [Mandal et al. \(2020\)](#), which does not keep track of the sunspot groups and thus the same group is recorded multiple times as independent observations. This means that if a group lives for a longer time (the big group), then it will be counted for a larger number than a shorter-lived group. To show that this weighting factor for the big groups does not affect our conclusion, we consider the sunspot data from Royal Observatory (RGO, Greenwich - USAF/NOAA), where the group numbers are recorded. By considering each sunspot group only once, we repeat our analyses. We find that the results remain qualitatively similar, and our conclusion remains unaltered.

This paper has been typeset from a $\text{\TeX}/\text{\LaTeX}$ file prepared by the author.

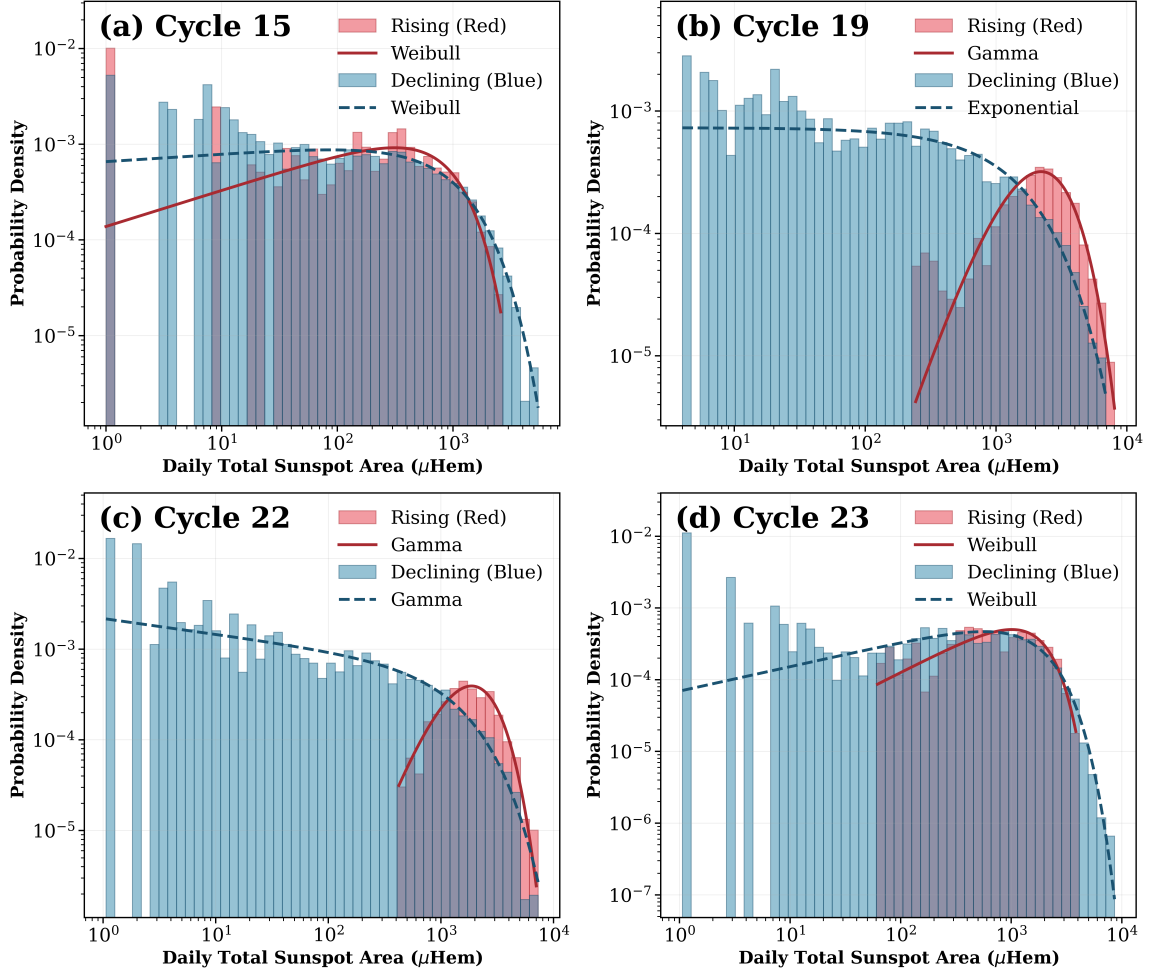


Figure A1. Distributions of the daily group sunspot area (in μHem) during the rising (red) and declining (blue) phases of Cycles 15, 19, 22 and 23.